INTERNATIONAL JOURNAL OF VENTILATION, 2016
http://dx.doi.org/10.1080/14733315.2016.1252146

Taylor & Francis
Taylor & Francis Group

Numerical study of the cross-ventilation of an isolated building with different opening aspect ratios and locations for various wind directions

Shahram Derakhshan and Ahmad Shaker

School of Mechanical Engineering, Iran University of Science & Technology, Tehran, Iran

ABSTRACT

Increasing the natural ventilation potential is an effective way to reduce energy consumption in buildings. In this paper, by using computational fluid dynamics (CFD), the natural ventilation of the wind flow was simulated to evaluate the affecting parameters on the volume flux in an isolated building. The studied parameters were the opening aspect ratios and their locations for various wind directions. Investigations were performed for seven window aspect ratios with the same opening area, six different wind directions, and eight different lateral- and vertical-positions on a leeward wall. The 3D steady Reynolds-averaged Navier–Stokes (RANS) equations were solved by a commercially available finite volume code. To provide closure, an SST $k - \omega$ turbulence model was coupled to the momentum equations to evaluate the Reynolds stresses. To validate the numerical method, the CFD results were compared with the numerical and experimental results obtained by other studies. A reasonable agreement was observed between the reference data and this study's results. These results showed that small changes, such as in the window dimensions or the lateral and vertical locations, affected the natural ventilation flow by increasing the volume flux. In addition, these results showed that when the wind direction was at an angle of more than 45°, the volume flow rate was approximately independent of the opening's dimensions.

KEYWORDS

Computational fluid dynamics (CFD); isolated building; natural ventilation; volume flux

1. Introduction

Presently, the energy consumption for heating, ventilation, and air conditioning (HVAC) systems is remarkable. A study conducted by Orme (2001) reports that 68% of the consumed energy in service and residential buildings is due to their HVAC systems.

The wind flow generated by the wind energy in urban environments has an effect on the distribution of heat and building pollution. Many researches are performed to improve occupants comfort, health, and work performance by different parameters sensitivity analysis. Hathway, Papakonstantis, Bruce-Konuah, and Brevis (2015) worked on air exchange and infection transfer in office and hospital buildings.

The developmental welfare of the residents has always been of interest for researchers and designers of buildings. A review of the internal building flow can assist in choosing the best plan. In addition, the reduction of energy consumption necessary for indoor air conditioning is one of the issues that has been considered in recent years. Using natural ventilation in buildings is one way to

CONTACT Shahram Derakhshan shderakhshan@iust.ac.ir

reduce the energy consumption necessary for building ventilation. The selection of a better building plan is possible when considering the project area's conditions, including the direction of the wind, the obstacles in the area, the way the obstacles are arranged, etc.

A project that requires lower energy consumption for indoor ventilation in the analysed area is a better building design.

Natural ventilation in a building can be implemented by single-sided or cross-ventilation. In single-sided ventilation, there is an opening in the windward or leeward wall, which allows the entering and existing air to flow through it. In cross-ventilation, the indoor flow is created from the flow between the entrance and exit of the front walls. Natural ventilation may be used in building by attaching system on building. Ghadiri, Lukman, and Mohamed (2013) studied the effect of usage the wind catcher on building in order to ventilating indoor air.

Semi-empirical relationships were presented for the ventilation rate of a building. The most common method is using the orifice equation to calculate the flow rate through the doors and windows of a building (Allard, 1998). In addition, dimensionless parameters have been presented for the calculation of the inlet flow rate (Linden, 1993; Chu, Chiu, Chen, Wang, & Chou, 2009; Etheridge 2012). Moreover, the density, pressure coefficient, discharge coefficient, the opening area in the windward and leeward walls and the pressure difference between the indoor and outdoor walls are important.

The efficiency of the single-sided or cross-ventilation process depends on the different parameters. The various directions of the wind flow, in the example of pollution dispersion, have been investigated by Rong, Liu, Pedersen and Zhang (2015), Liu, Niu, and Kwok (2011), and Saha et al. (2013).

The existence of obstacles in a building has an effect on the inlet volume flux of the building. According to an evaluation on the impact of the obstacles, a resistance factor can be defined to be a function of the discharge coefficient and the inlet and outlet opening areas.

Chu and Chiang (2013) considered a vertical obstacle in the middle of a building in their model. Their results showed that the resistance factor depends on the position and size of the obstacle, but is independent of the wind speed outside the building, the dimensions of the building and the placement of the windows.

Chu, Chiu, and Wang (2010) considered an isolated building that was divided by a partition wall into two separate parts. Their investigation showed that the internal discharge coefficient depends on the opening area of the partition wall and does not depend on the inlet and outlet opening areas or the locations of the windows and doors. In comparison with non-obstacle buildings, the reduction of the pressure difference between the indoor and outdoor building flows caused the ventilation rate to decrease.

The external geometry of the building is one factor that has an important role in determining the indoor and outdoor flows of the building. Montazeri and Blocken (2013) worked on buildings with and without balconies. Their results suggest that a balcony can lead to severe changes in the air pressure distribution, as much as 30% in some areas.

Several studies have been conducted on the influence of the building's roof on the wind flow rate. Tominagaa, Akabayashib, Kitaharaa and Arinamib (2015) analysed the shape of the roof with three various gable-roof building models. Peren, van Hooff, Leite, and Blocken (2015) also considered the influence of the roof inclination on the inside and outside flow parameters.

Yu, Xie, and Gu (2015) simulated the interaction between two neighbourhood buildings with different arrangements. Tominaga and Blocken (2015) investigated their model in single and multiple isolated buildings.

Wall porosity (i.e. the size of the openings) is an important parameter that affects the pressure distribution of the building interval and has been investigated by some researchers (Karava, Stathopoulos, & Athienitis, 2004; Karava, Stathopoulos, & Athienitis, 2006; Karava, Stathopoulos, & Athienitis, 2011; Karava & Stathopoulos, 2012).

The numerical results obtained by Chu and Chiang (2014) showed that an increase in the building length caused a reduction in the pressure difference between the windward and leeward walls and consequently the ventilation rate. Chu and Chiang (2014) investigated a typical model where the

inlet and outlet doors where not exactly facing each other. This change in location caused a lower ventilation rate than when the doors were located in front of each other.

Jesson, Sterling, Letchford, and Baker (2015) investigated the aerodynamic force and pressure coefficient distribution on the roofs of low, mid- and high-rise buildings.

Natural ventilation is caused by buoyancy and the wind force. The pressure difference around the building is created by these two driving forces. The shape of the window and its dimensions contribute to the pressure distribution on the walls of the building. Many studies have been performed to better understand the interaction of these two forces. For example, the results provided by Allocca, Chen, and Glicksman (2003) show that under certain conditions, the impact of the buoyancy force is greater than the wind force when the ventilation rate produced solely by the buoyancy force is higher than the rate caused by the wind force. In other researches, buoyancy-driven natural ventilation in ventilation shafts is investigated by Stephen and Leon (2013) in office building. Also, Andersen (2015) reported semi-empirical models for buoyancy-driven ventilation in rooms at four different types.

Researchers have used experimental and numerical methods to investigate the indoor and the outdoor flows of a building. The experimental studies on inside building flow are based on a full-scale model (Jiang, Alexander, Jenkins, Arthur, & Chen, 2003; Wong & Hand Heryanto, 2004) or a small-scale model (Karava, 2008; Lee et al., 2005). The possibility of using a wind tunnel in small-scale models allows for easier control of the operating conditions, such as wind speed and direction. Therefore, this experimental approach is preferred over full-scale models.

Two numerical methods are used to study natural ventilation: the coupled and decoupled approaches. In the decoupled approach, the outdoor flow and the indoor flow are studied in two separate discrete models (Jiang & Chen, 2002), but in the coupled approach, they are studied simultaneously.

Inefficiency in the decoupled approach is caused by the dissipation of the turbulence kinetic energy on the windward wall and ignoring the effect of the dynamic pressure of the airflow passing through the opening area (Murakami, Kato, Akabayashi, & Kim, 1991; Etheridge & Sandberg, 1996; Seifert, Li, Axley, & Rösler 2006). Recently, in natural ventilation research, the coupled approach has been used rather than the decoupled approach.

Researchers have used various turbulence models, such as the large eddy simulation (LES) model and the RANS model. A comparison of the RANS model results with the experimental results showed that this model has an acceptable accuracy for the natural ventilation in isolated buildings. More data are available for the RANS model (Mistriotis, Bot, Picuno, & Scarascia-Mugnozza, 1997; Jiang & Chen, 2001; Fatnassi, Boulard, Poncet, & Chave, 2006, Bartzanas, Kittas and Nikita-Martzopoulou, 2007; Larsen, Nikolopoulos, Nikolopoulos, Strotos, & Nikas, 2011) than for the LES model (Kato, Murakami, Mochida, Akabayashi, & Tominaga, 1992; Jiang et al., 2003; Hu, Ohba, & Yoshie, 2008).

In this study, the changes in the window dimensions, the lateral and the vertical locations of the openings, and different wind directions with different window aspect ratios have been investigated to determine the effect of these parameters on natural ventilation. Numerical simulations were performed using the 3D steady state of the Reynolds-averaged Navier–Stokes (RANS) equations. The coupled approach was used to solve the indoor and outdoor building airflow analysis simultaneously. The results of the experimental studies by Karava (2008) and Ohba, Irie and Kurabuchi (2001) and also the numerical study by Chu and Chiang (2014) were used to validate the results of this research. The presented results consisted of the airflow patterns and the volume flow rates obtained from CFD analysis.

2. Numerical setup

2.1. Computational domain and grid generation

A CFD simulation was performed on a reduced scale (1:200) model. The dimensions of the domain were selected by the guidelines of Franke et al. (2007), Tominaga et al. (2008) and Van Hooff and Blocken (2010). These dimensions can be observed in Figures 1 and 2 as well as Table 1.

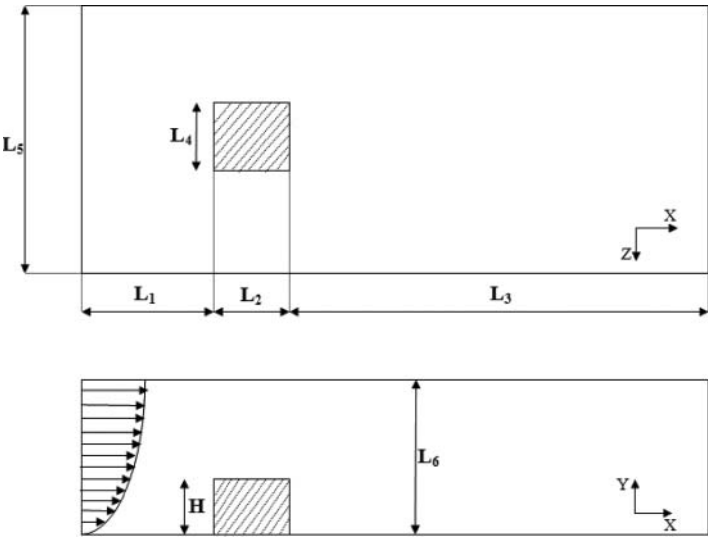

Figure 1. Computational domain.

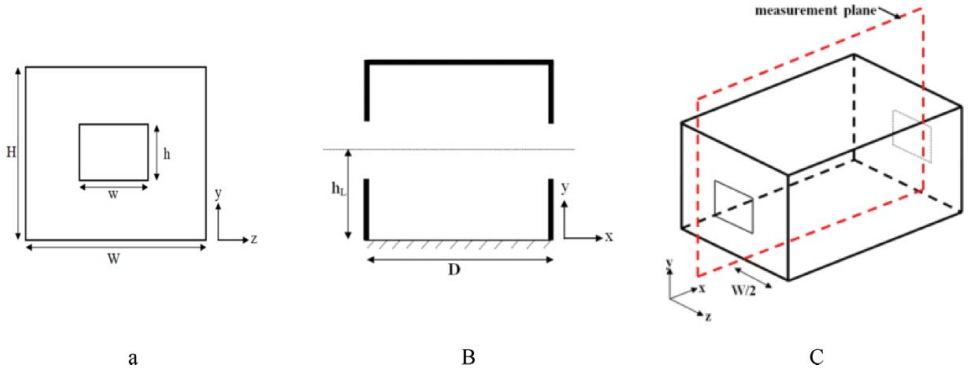

Figure 2. (a) Window and building dimensions at windward and leeward wall of the building. (b) Vertical cross-section of the building model. (c) Position of the measurement plane in building model.

The dimensions of the domain are width X depth X height = 0.9 X 1.54 X 0.48 m^3, which correspond to the dimensions of 180 X 308 X 96 m^3 for the full-scale model. In addition, the reference case used has a reduced scale model with dimensions of 0.1 X 0.1 X 0.08 m^3, which correspond to $20 \times 20 \times 16$ m^3 in the full-scale dimension. For cases when the wind directions are not zero, such as in the study by Montazeri and Blocken (2013), the dimensions can be seen in Table 1.

The computational grid for the domain was fully structured. The Van Hooff and Blocken (2010) technique was used for creating the grid because it has full control over the size and shape of every cell in the grid. The stretching ratio around the building was under a value of 1.2. To investigate the

Table 1. Dimensions of computational domain.

Title	Dimension for 0° wind direction	Dimension for non-zero wind direction
L_1	3H	3H
L_3	15H	15H
L_5	L_4+10H	L_4+18H
L_6	6H	6H

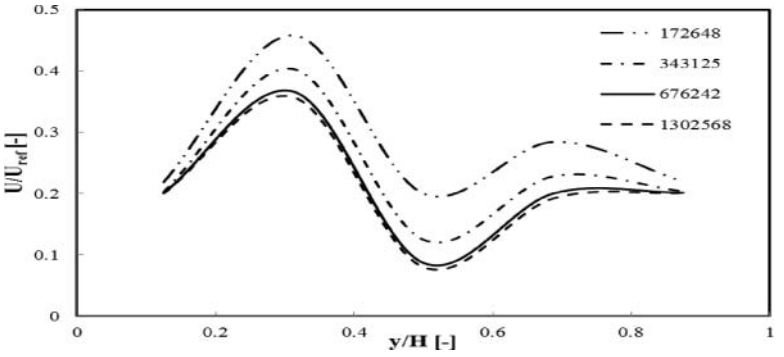

Figure 3. Comparison of the streamwise wind speed ratio (U/U_{ref}) along the vertical line in measurement plane at middle of the building model for four grids.

mesh independency, according to Patankar and Suhas (Patankar 1980), the number of cells in the grids for the four models were doubled. Figure 3 compares the streamwise wind speed ratio (U/U_{ref}) along the vertical line in the measurement plane at the middle of the building model for the four grids. The results indicated that the usage of over 676,242 cells has nearly the same results for all four grids. Therefore, this numbers of cells is suitable for a CFD simulation. Figure 4 shows the 3D computational grid.

2.2. Geometry of the models

There were two windows in the reference case with dimensions of 0.046 X 0.018 m^2, and these windows were placed at the middle of the windward and leeward walls ($h_L = 0.04$ m). For other simulation models in this paper, the window dimensions have been changed by the frozen opening area of the reference model. Table 2 and Figure 5 represent the dimensions of the different windows, where r_a is the ratio of the width to the height of the window as follows:

$$r_a = \frac{w}{h}. \tag{1}$$

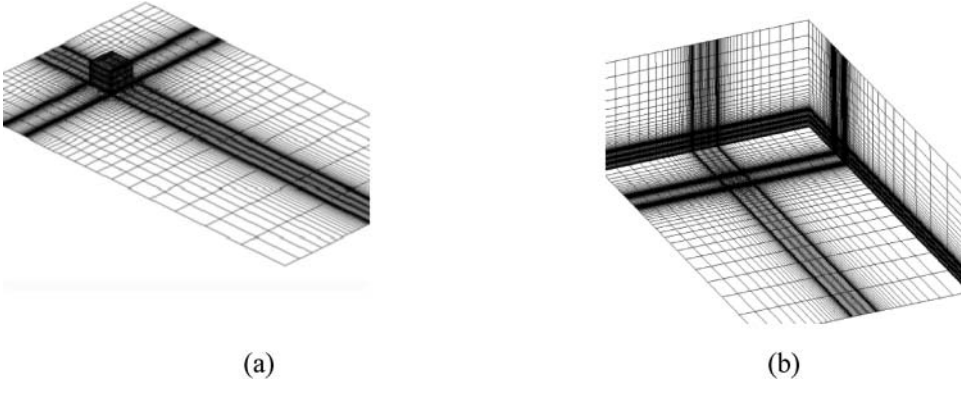

Figure 4. Computational grid: (a) grid at building surfaces and ground surface; (b) grid at bottom and lateral faces of computational domain.

Table 2. Dimension of different windows.

Width × height (mm^2)	r_a(–)
18 × 46	0.39
23 × 36	0.64
28.8 × 28.8	1.00
30 × 27.6	1.09
36 × 23	1.56
40 × 20.7	1.93
46 × 18	2.55

2.3. Boundary condition

To impose the inlet boundary condition on the numerical simulation, it is necessary to use the measured vertical profiles of the mean wind speed U and the streamwise turbulence intensity. The logarithmic law was used to define the inlet profile of the mean wind speed as follows:

$$U(z) = \frac{u*}{k} \ln\left(\frac{z + z_0}{z_0}\right), \tag{2}$$

where u^* is the friction velocity (=0.35 m/s) defined based on the values of the experiment, $\kappa = 0.42$ is the Von Karman constant, z_0 is the aerodynamic roughness length, and z is the coordinate height.

In wind tunnel testing, the incident vertical profiles of the mean wind speed and the streamwise turbulence intensity were measured by particle image velocimetry (PIV) (Karava 2008). In Figure 6(a), the incident vertical profiles of the mean wind speed, the streamwise turbulence intensity measured in the mentioned process, and the logarithmic inlet profile of the mean wind speed are illustrated.

The general equation for the turbulent kinetic energy is determined by

$$k(z) = a\left(I_U(z)U(z)\right)^2, \tag{3}$$

where $a = 0.5$, 1.0, or 1.5 (Ramponi and Blocken, 2012a).

In this paper, according to Tominaga et al. (2008) recommendations and Ramponi and Blocken (2012b) proof, the value of 1.0 is used for a.

The streamwise turbulence intensity is related to the standard deviation of the turbulent fluctuations as follows:

$$I_U(z) = \frac{\sigma}{U}. \tag{4}$$

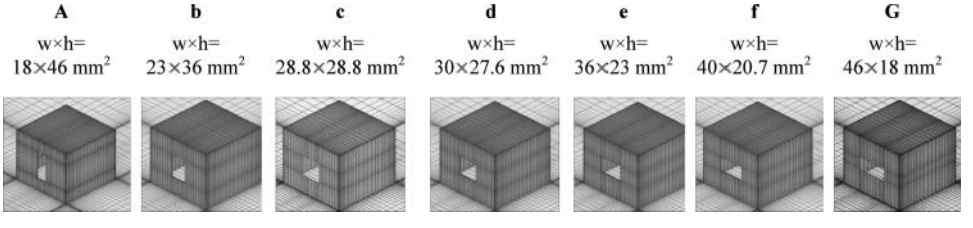

Figure 5. Computational grid for building with different window dimension ratio. (a) $r_a = 0.39$; (b) $r_a = 0.64$; (c) $r_a = 1$; (d) $r_a = 1.09$; (e) $r_a = 1.56$; (f) $r_a = 1.93$; (g) $r_a = 2.55$.

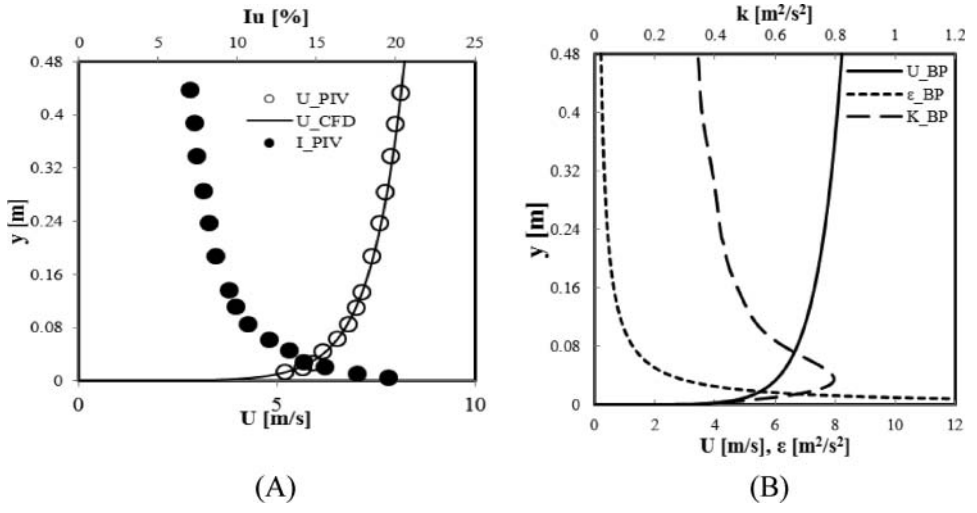

Figure 6. (a) Incident vertical profiles of mean wind speed and streamwise turbulence intensity, (b) incident profiles of mean wind speed (U), turbulent kinetic energy (k), and dissipation rate (ε) at the building position used in CFD simulations.

The vertical profile of the turbulence dissipation rate is as follows:

$$\varepsilon(z) = \frac{u^{*3}}{k(z+z_0)}. \tag{5}$$

By controlling the amount of turbulent kinetic energy and the turbulence dissipation rate, the specific dissipation rate can be computed as follows:

$$\omega(z) = \frac{\varepsilon(z)}{C_\mu k(z)}, \tag{6}$$

where C_μ =0.09 is an empirical constant.

To apply the wall functions at the ground and building surfaces, a combination of the standard wall functions developed by Launder and Spalding (1974) and the sand-grain based roughness modification developed by Cebeci and Bradshaw (1977) were used.

Blocken, Carmeliet and Stathopoulos (2007) presented an equation that relates the sand-grain roughness height (k_s), the roughness constant (C_s), and the aerodynamic roughness length (z_0) parameters as follows:

$$k_s = \frac{9.793 z_0}{C_s}. \tag{7}$$

Based on Equation (7), the value of the roughness parameter was 0.28 mm, and the roughness constant was 0.874 for the ground surfaces. For the building surface, the value of the roughness parameters imposed was zero.

To approach a real situation for the airflow of a building, the incident profiles were used instead of the inlet profiles. The incident profiles were obtained as detailed by Blocken, Stathopoulos and Carmeliet (2007). These profiles appear at the building position in the empty domain of the simulation. Figure 6(b) shows the incident profiles of the mean wind speed (U), turbulent kinetic energy (k), and specific dissipation rate (ω) at the building position.

The symmetry boundary conditions were used for applying the zero normal velocity and the zero normal gradients of all variables at the top, right, and left sides of the domain. Zero static pressure was defined for the outlet side of the domain. For the cases with a non-zero wind direction, the inlet boundary condition was determined for the left side, and the zero static pressure was applied on the right side with the other boundary conditions unchanged.

2.4. Solver settings

The commercially available finite volume code ANSYS FLUENT 12 (2009) was used for the CFD simulations. The 3D steady-state Reynolds-averaged Navier–Stokes (RANS) equations and the (SST) $k-\omega$ turbulence model (Menter, 1994) were solved by the performed numerical simulations. The SIMPLE algorithm was used for the pressure-velocity coupling. Second-order discretisation schemes were used for the convection and viscous terms in the governing equations. In addition, the pressure was derived by the second-order interpolation. All the scaled residuals converged and reached a minimum of 10^{-4} for ω with continuity, 10^{-5} for k, and 10^{-6} for the x-, y- and z-velocities, which were considered as the convergence criteria. When the simulations achieved oscillatory convergence, the results were monitored over 10,500 iterations, and the values of the variables were determined by averaging the last 500 iterations (i.e. iterations 10,000–10,500).

Figure 1 demonstrates oscillatory behaviour for scaled residuals monitored over the first 10,000 iterations for reference case (Figure 7(a)) and for pressure coefficient monitored over 10,000 iterations in three selected points along the centreline for model (Figure 7(b)). Equality of values for point 1 and small oscillations in points 2 and 3 shows that the value of pressure coefficient is acceptable.

3. Validation of the CFD simulation

The experimental study performed by Ohba et al. (2001) was used to validate the wind direction. The test section of the wind tunnel used by this group had dimensions width $\times$ height $\times$ depth $=$ 1.2 $\times$ 1 $\times$ 14 m^3, and the dimensions of their model were 0.3 $\times$ 0.15 $\times$ 0.3 m^3. Figure 8 shows the obtained results from this study's numerical simulation in comparison with the cited experimental study. The deviation between the numerical and experimental results ranged from 1% to 9%.

In another experimental study on an isolated building, a small-scale model with dimensions of 0.1 $\times$ 0.08 $\times$ 0.1 m^3 was placed in a wind tunnel that had dimensions of 1.8 $\times$ 1.8 $\times$ 12 m^3 [17]. Chu and Chiang (2014) used an LES model to study the wind driven cross-ventilation. Their model had the same dimensions used by Karava (2008). In Figure 9, the mean velocity in the vertical centre plane and the streamwise wind speed ratio along the connecting line between the window centres are shown based on this study's numerical simulation results and the data reported by Karava (2008) and Chu and Chiang (2014). Despite the differences in some results, overall, the results are in fairly good agreement.

4. Results and discussion

4.1. Impact of a window's width and height

In Figure 10, different values of the ventilation rate for different window dimensions with a wind angle of 0° have been presented. The reference volume flux has been used to calculate the dimensionless group for the volume flux of the building inlet as follows:

$$Q_{ref} = w \times h \times U_{ref} = 0.023 \times 0.036 \times 6.97 = 0.00577 \ m^3 \ s^{-1}. \quad (8)$$

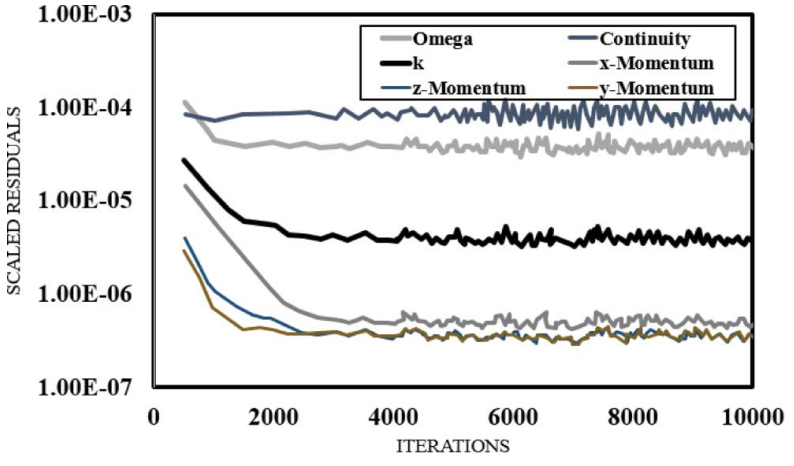

(a)

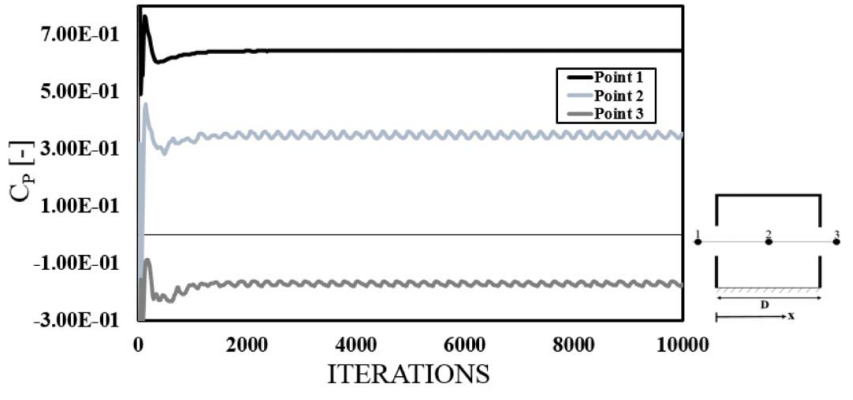

(b)

Figure 7. Oscillatory behaviour: (a) scaled residuals monitored over the first 10,000 iterations for reference case; (b) pressure coefficient monitored over 10000 iterations in three selected points along the centerline for model with $r_a = 0.64$: upstream of the inlet opening ($x/D = -0.2$); in the center of the building ($x/D = 0.5$) and downstream of the outlet opening ($x/D = 1.2$).

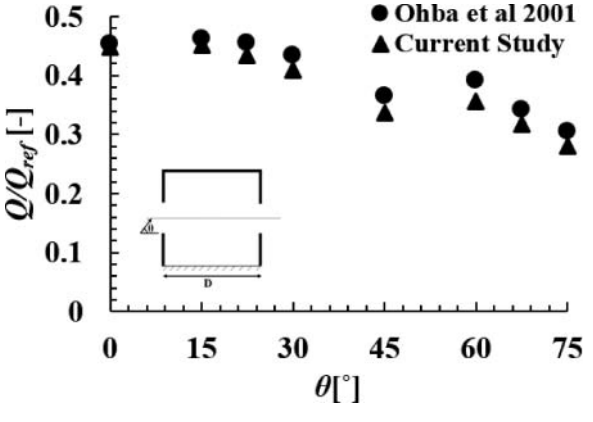

Figure 8. Comparison of numerical and experimental volume flow rate Q/Q_{ref}

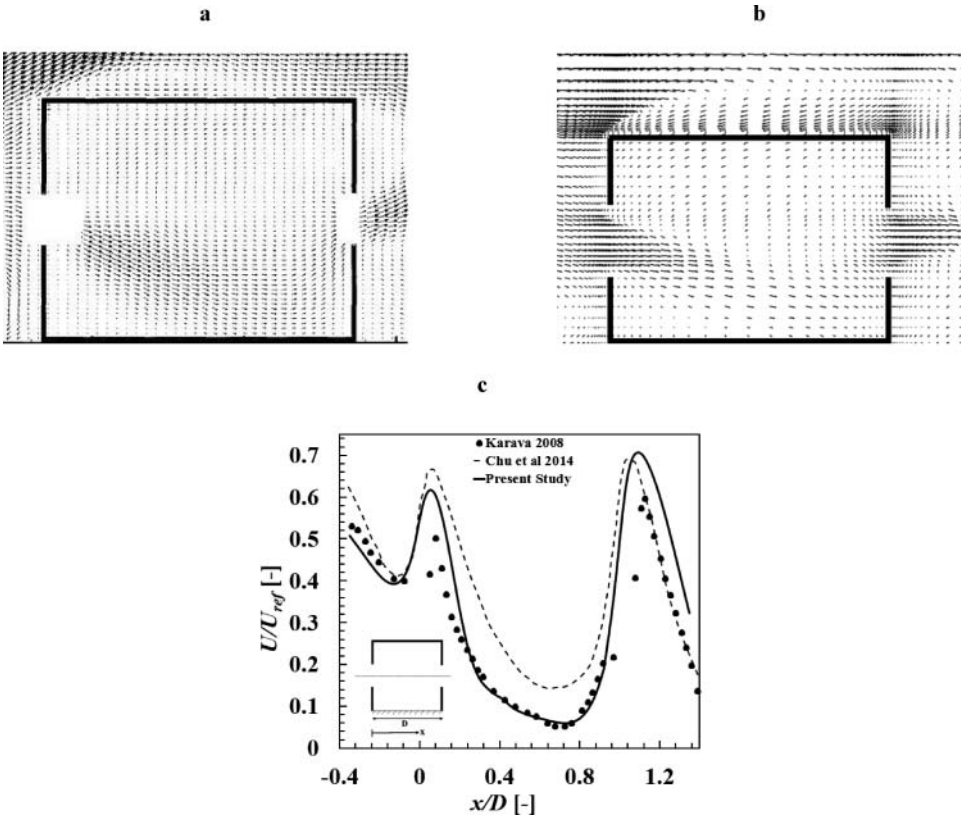

Figure 9. Comparison of the mean velocity in the vertical center plane obtained from: (a) Karava (Karava 2008); (b) present numerical simulation; (c) comparison of streamwise wind speed ratio U/U_{ref} along the connecting line of window centers processed from present study and Chu et al (Chu et al. 2014) and Karava (Karava 2008)

The results in Figure 10 indicate that the maximum amount of inlet air occurs at $r_a = 0.5$, and the minimum amount occurs at $r_a = 2.5$. Generally, increasing the width-to-height ratio reduces the volume flux.

To increase the ventilation rate of the building, rectangle windows are used rather than square ones. For $0.8 < r_b < 1.2$, the ventilation rate becomes very low, and the lowest value of the ventilation rate occurs at $r_a = 1.0$. Comparing the results for windows with different r_a ratios indicated that the greatest impact of the changing parameter r_a on the ventilation rate was approximately 10%. Among

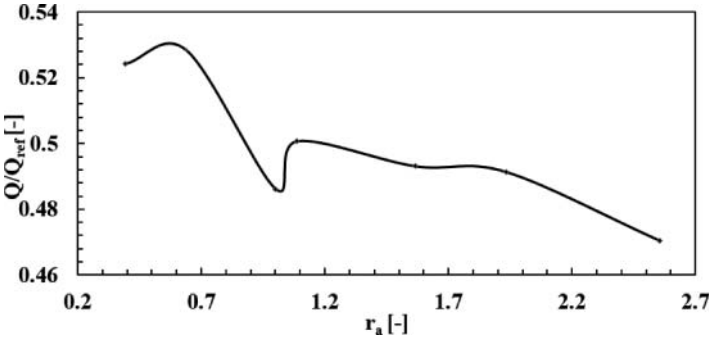

Figure 10. The value of Q/Q_{ref} for different window dimensions with wind direction 0°.

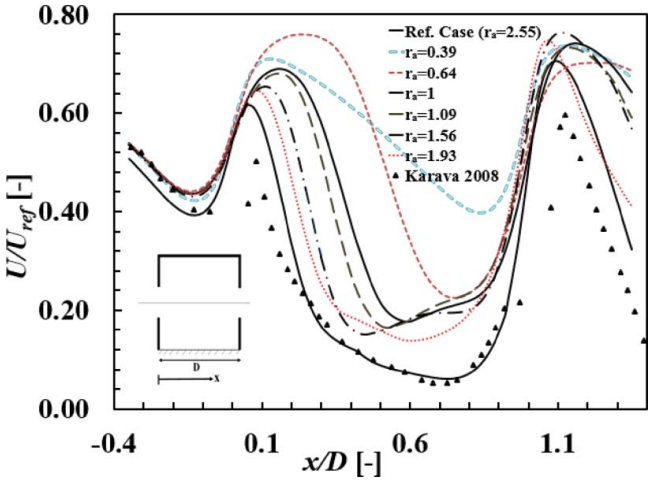

Figure 11. Comparison of streamwise wind speed ratio U/U_{ref} along horizontal line for different value of r_a.

the different dimensions of windows used in this research, the window with dimensions of width × height = 23 × 36 m^2 had the highest volume flux.

The streamwise wind speed ratio U/U_{ref}, which is along the line that joins the windows centres together in the horizontal centre plane, has been plotted for different values of r_a in Figure 11. In addition, in this figure, the current numerical results have been compared with the data reported by Karava (2008). In the zone at the front of the windward window ($\frac{x}{D} < 0$), the streamwise wind speed ratio is almost independent of r_a. Actually, the obtained results in the different models are similar to the experimental data. In this region, the value of the streamwise wind speed ratio was first reduced, but then it increased due to changing conditions of the cross-section of flow. In the interior of the building ($0.2 < \frac{x}{D} < 1.0$), the changes of the streamwise wind speed ratio were the same for different values of r_a, and in the back of the windward window of the building, due to a sudden increasing in the cross-section of flow, the streamwise wind speed ratio sharply decreased. In the middle of the building ($0.4 < \frac{x}{D} < 0.8$) because of no change in the cross-section of flow and a constant flow rate, the streamwise wind speed ratio was almost constant for a certain value of r_a. Close to the window on the front of the leeward wall in the interior of the building ($0.8 < \frac{x}{D} < 1.0$), the stream wise wind speed ratio increased due to the window effect, and in the back of the leeward wall ($\frac{x}{D} > 1.0$), it was reduced.

Using windows with different dimensions, the back of the windward window in the interior of the building ($0.2 < \frac{x}{D} < 0.8$) was more affected than other parts of the indoor and outdoor walls of the building. Furthermore, by increasing the value of r_a, the streamwise wind speed ratio was reduced, and consequently, the volume flow rate was also reduced.

The contours of the pressure coefficient and of the velocity magnitude in the vertical centre plane have been shown for windows with different values of r_a in Figure 12. The pressure coefficient is determined as follows:

$$C_p = \frac{P - P_0}{0.5(\rho U_{ref}^2)}, \tag{9}$$

where P is the static pressure, P_0 is the reference static pressure, ρ is the air density (=1.225 kg/m^3), and U_{ref} is the velocity at the building height (=6.97 m/s).

The difference of the various contours is seen on the region between the front of the windward windows and the back of the leeward windows. This difference is due to the change in the height of

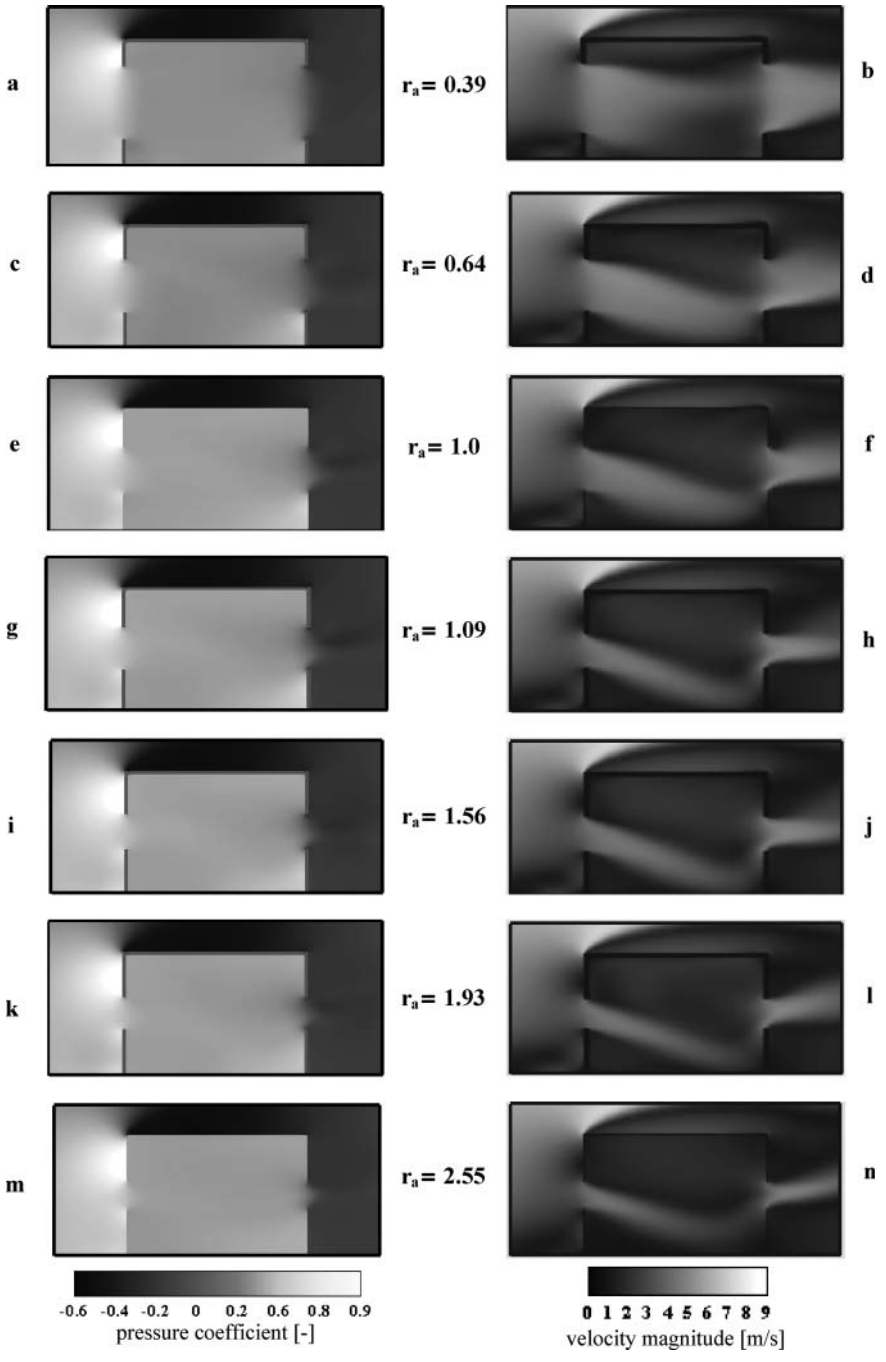

Figure 12. (a, c, e, g, l, k, m) Contours of pressure coefficient in vertical center plane for different r_a. (b, d, f, h, j, l, n) Contours of velocity magnitude in vertical center plane for different r_a.

the windows. In the indoor building environment, by increasing the height of the windows, the area for regions with high wind speeds reduces, and the area for the regions with low wind speeds increases. In addition, in all models, the maximum speed is created at the leading edge of the roof.

The comparison of different contours of the pressure coefficient shows that by increasing the height of the window, the pressure coefficient changes will be reduced in the indoor building

Table 3. Dimensionless area-averaged velocity magnitude ($|V|/U_{ref}$) in the occupied zone in the vertical plane for different r_a.

	$\lvert V\rvert/U_{ref}$		
	Entire occupied zone	Lower part	Upper part
$r_a = 0.39$	0.64	0.61	0.75
$r_a = 0.64$	0.70	0.70	0.66
$r_a = 1$	0.47	0.49	0.37
$r_a = 1.09$	0.37	0.38	0.29
$r_a = 1.56$	0.36	0.37	0.29
$r_a = 1.93$	0.34	0.35	0.26
$r_a = 2.55$	0.31	0.33	0.21

environment. Pressure differences in the front of the windward wall are higher than behind the leeward wall for different models. These results suggest that the dimensions of the window are an important parameter to increase the volume flow rate.

The dimensionless area-averaged velocity magnitude can be used to further investigate the patterns created for different dimensions of a window. The mentioned velocity is calculated in the occupied zone for the vertical plane. This area ranges from the ground to the top of the window of the reference model. The mentioned zone is the most important building area due to its residents. Table 3 shows the dimensionless area-averaged velocity magnitude for different values of r_a. In this table, the differences of the calculated values indicate the impact of the window dimensions on the indoor flow pattern. The maximum difference between these values for different models is approximately 55%.

The use of windows with a greater height caused a significant increase in the dimensionless area-averaged velocity magnitude in the occupied zone for the vertical plane. The changing process indicates that for certain porosities, the occupied zone is more affected by the use of squared windows or by windows with a larger height than width. The calculated velocity in the occupied zone for the vertical plane for models with $r_a \leq 1$ is higher than for other models.

The indoor building zone can be more accurately analysed by dividing this zone into lower and upper regions. The lower region ranges from the ground floor to the middle height of the reference model window, and the upper region ranges from the middle height of the reference model window to the top of the building. Using different window dimensions, the upper region is more affected than the lower region. For the cases with $r_a > 1$, the flow entering through the inlet opening is directed to the lower region of the building, and by decreasing the value of r_a, the upper region is more affected by the inflow.

The pressure difference around the building is one of the important parameters of natural ventilation. Figure 13 shows the values of the pressure coefficient along the centreline of the vertical plane. Pressure losses in the inlet and outlet openings caused a reduction in flow pressure.

Generally, the flow pressure in the interior space was uniform for all models. The pressure dramatically decreased in models with rectangular windows with an aspect ratio less than 1.0 because of a strong vortex in the building inlet. Pressure losses in the outlet section for models with $r_a > 1.0$ were greater than those with $r_a < 1.0$. This fact aids in increasing the inlet flow rate of buildings with $r_a < 1.0$.

4.2. Impact of the wind direction

In this section, the effect of the wind direction on the ventilation rate is investigated. In Figure 14, the ventilation rate changes for different wind directions with different values of r_a are depicted.

These results showed that for angles greater than 20°, the rate of the volume flow decreased significantly when the wind angle increased. A significant change was not observed for wind angles less than 20° for a given r_a. The rate of ventilation observed at angles ranging from 0° to 30° is magnified in Figure 14(b). The results in this section show that the highest ventilation rate occurs with a 0° wind angle and $r_a = 0.64$. Therefore, for different values of r_a, the maximum ventilation rate occurs at

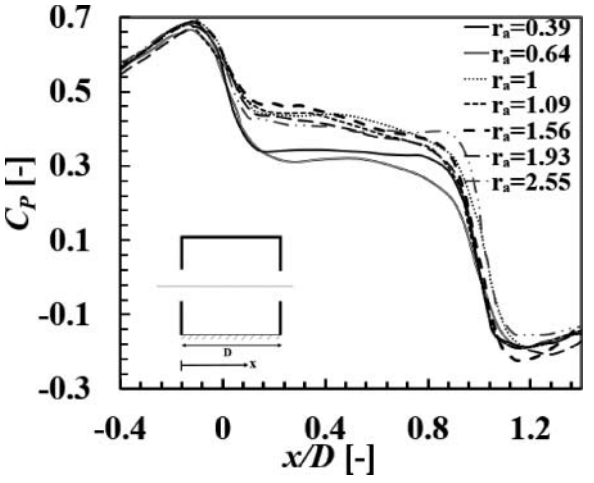

Figure 13. Pressure coefficient along the horizontal line in vertical plane.

angles ranging from 0° to 15°. In addition, for different window dimensions with a wind direction greater than 45°, the volume flux is independent of the window size.

Figure 2(a, c, e, g, i) shows pressure coefficient counters at the centre of window height in different wind direction for $r_a = 0.64$ and Figure 2(b, d, f, h, j) and velocity magnitude contours at the centre of window height in different wind direction for $r_a = 0.64$. It is clear that high pressure and low pressure zones of domain are changed for various wind directions. Higher wind directions leads to a wide high pressure domain in front wall. Therefore, the inlet flow rate increases.

4.3. Impact of the window location

According to Section 4.1, the window dimensions width × height = 23 × 36 mm^2 has the highest volume flux in all the cases used in this study. Therefore in this section, the models were studied to evaluate the changing impact the window location has for a window with dimensions 23 × 36 mm^2. In this section, increasing the ventilation rate was obtained by changing the location of the window.

As Figure 16 illustrates, the value of the disposition of the window centre along the *z*-axis and the *y*-axis are termed Δw and Δh, respectively. The horizontal changes, Δ*w*, are equal to 0.05 W, and in

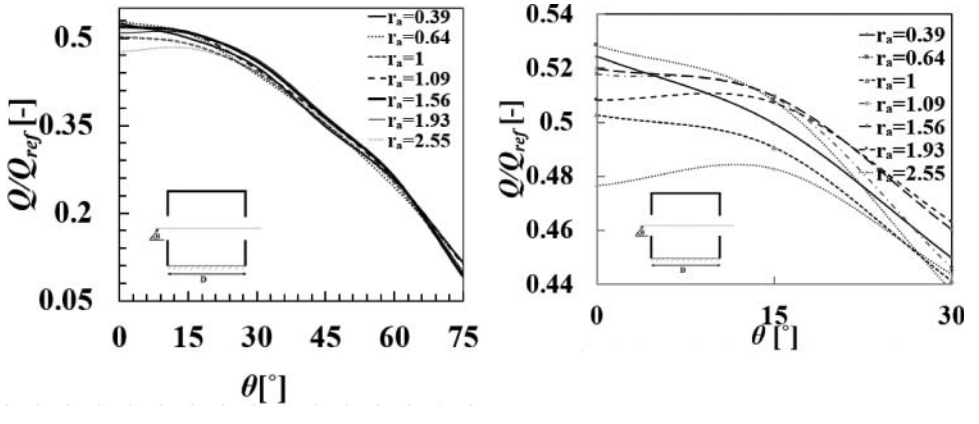

Figure 14. Value of Q/Q_{ref} for different wind direction with different window dimensions, wind direction $0° < \theta < 75°$ (left) and wind direction $0° < \theta < 30°$ (right).

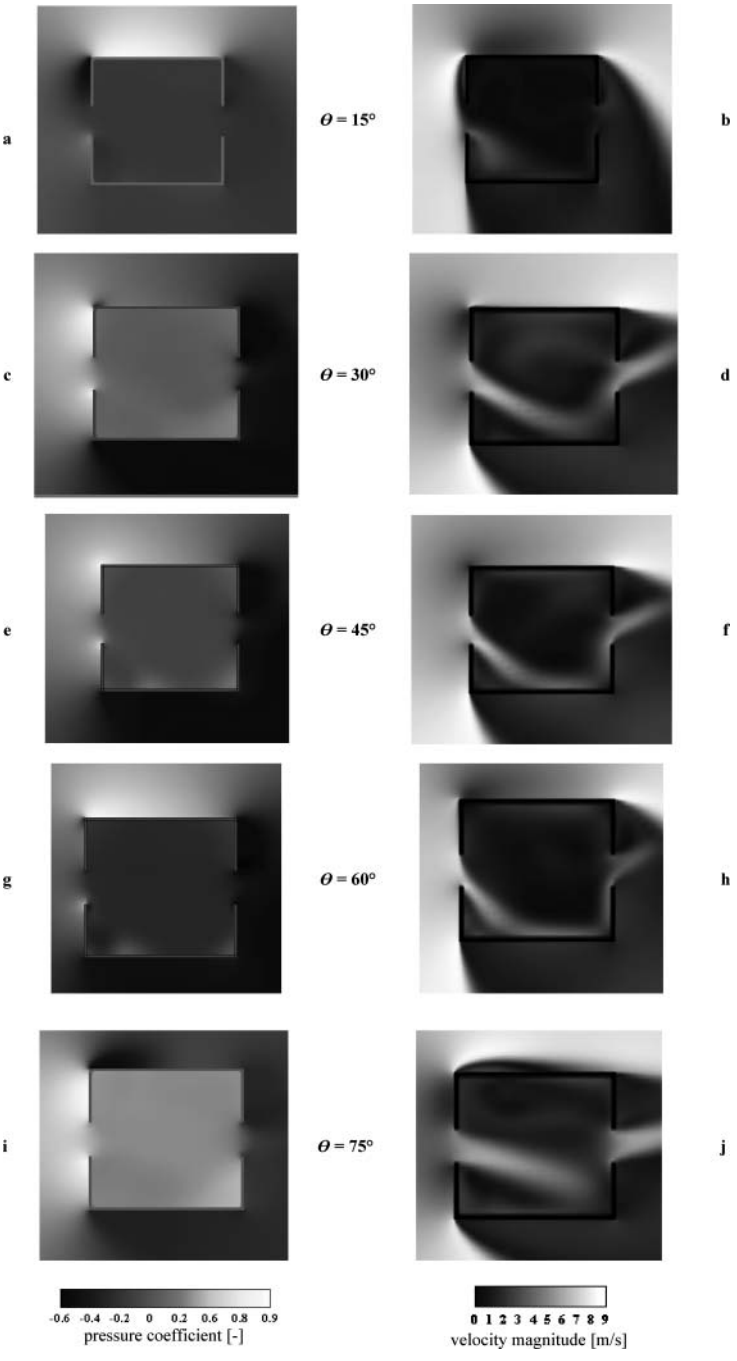

Figure 15. (a, c, e, g, i) Contours of pressure coefficient at the centre of window height in different wind direction for $r_a = 0.64$; (b, d, f, h, j) Contours of velocity magnitude at the centre of window height in different wind direction for $r_a = 0.64$.

the height changes Δh are equal to 0.0625H. It is necessary to mention that in models where the horizontal position was changed, the vertical position was fixed at the middle of the wall and vice versa.

Figure 17(a) refers to the impact of horizontal changes on the ventilation rate. All of these changes have a positive effect on the volume flux. The obtained volume flux for the different models studied

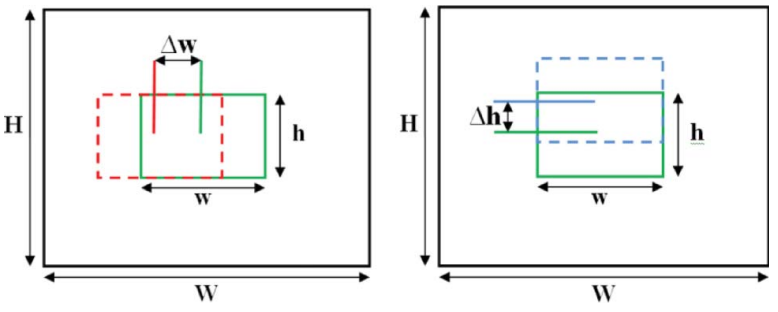

Figure 16. Value of disposition of the window center along *z*-axis, named "Δ*w*" and "Δ*h*" along *y*-axis.

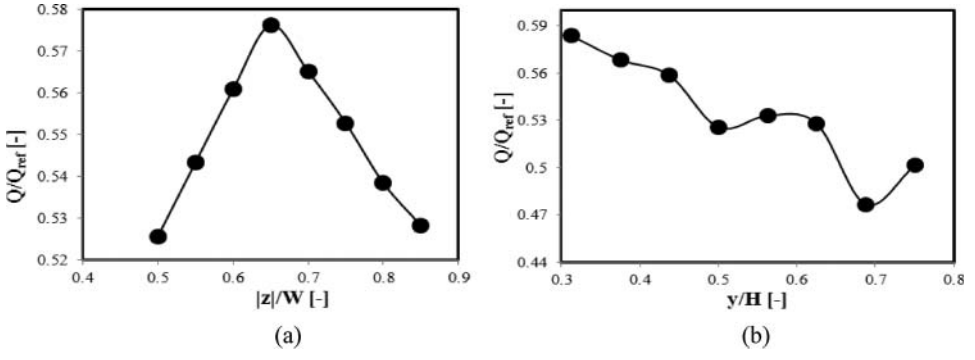

Figure 17. (a) Influence of horizontal position of the leeward window on the volume flux. (b) Influence of vertical position of the leeward window on the volume flux.

in this section showed an extreme improvement of approximately 9% relative to the non-dislocated model. The greatest ventilation rate can be observed in the range of $0.6 < \frac{|z|}{W} < 0.7$.

In Table 4, the given improvement of the ventilation rate for different horizontal dispositions is relative to the reference case. The results show a positive effect of the horizontal position of the window on the leeward wall from the middle to the lateral side of the wall. According to the data in Table 4, this change led to an increase of the ventilation rate of approximately 22.5%.

Figure 17(b) shows the influence of the vertical location of the window on the building inlet volume flux. The results reported in this figure show that the volume flux increases when the vertical location of window is lower than the middle height of the building. By placing the window between the middle of the building and a vertical location of y/H = 0.65, the volume flux remained almost fixed. The volume flux was reduced when the window was located higher than the mentioned location. Locating the window under the middle height of the building increased the volume flux, while

Table 4. The improvements offered by width position changes of the leeward window.

$\|z\|/W$	$Q_{CFD} \times 10^3$ ($m^3\ s^{-1}$)	$Q_{ref.\ case} \times 10^3$ ($m^3 s^{-1}$)	Improvement (%)
0.5	3.03	2.714	11.73
0.55	3.13		15.49
0.6	3.24		19.22
0.65	3.32		22.49
0.7	3.26		20.14
0.75	3.19		17.51
0.8	3.11		14.45
0.85	3.05		12.28

Table 5. The improvements offered by vertical position changes of the leeward window.

y/H	$Q_{CFD} \times 10^3$ ($m^3\ s^{-1}$)	$Q_{ref.\ case} \times 10^3$ ($m^3\ s^{-1}$)	Improvement (%)
0.3125	3.37	2.714	24.11
0.375	3.28		20.84
0.4375	3.22		18.78
0.5	3.03		11.73
0.5625	3.08		13.32
0.625	3.05		12.25
0.6875	2.75		1.33
0.75	2.89		6.59

the volume flux decreased when the window was placed over the middle height of the building. This mentioned increase was approximately 11% in comparison with the non-dislocated window.

Table 5 shows the improvement of the volume flux for different vertical locations of the window. Locating the window at $y/H = 0.3125$ increased the volume flux by approximately 24% in comparison with the reference case.

5. Conclusions

The parameters studied in this paper include the opening aspect ratios and their locations for various wind directions. The investigations were performed for seven window aspect ratios with an equal opening area, six different wind directions, and eight different lateral- and vertical-positions on the leeward wall. The 3D steady Reynolds-averaged Navier–Stokes (RANS) equations were solved by CFD to determine the results. The validation was performed by numerical and experimental results obtained from different studies. The results obtained in the different sections were as follows:

1. The change of the opening dimensions with a constant wall porosity (10%) indicated that the volume flow rate and the streamwise wind speed ratio depend on the window dimensions. Generally, the volume flux was reduced by increasing the width-to-height ratio. In addition, using a rectangular window rather than a square window increased the volume flow rate.
2. The investigation of the variation of the dimensionless area-averaged velocity magnitude showed that the outlet flow rate from the occupied zone for models with square windows or models with windows with an aspect ratio less than 1.0 are affected equally by the porosity. The maximum variation of the mean velocity is almost 55%.
3. Applying different wind directions to different window dimensions showed that the maximum volume flow rate occurred for angles ranging from 0 to 15°. For wind angles greater than 20°, the rate of volume flow decreased significantly. In addition, for different window dimensions with a wind direction greater than 45°, the volume flux was independent of the window size.
4. The positive impact by the increasing volume flow rate at the leeward window location changed in horizontal and vertical positions, which indicated that these changes can increase the mentioned rate. In addition, the volume flow rate was increased by approximately 24% in comparison with the reference case and by approximately 11% in comparison with non-dislocated window case.

For future research, non-isothermal conditions can be discussed to study the influence of the buoyancy force as one of the driving forces on natural ventilation. Furthermore, the effect of the window dimension changes will be considered in the crowd zone. In addition, the effect of the parameters such as width, height and length of the building with different wind direction should be studied.

Disclosure statement

No potential conflict of interest was reported by the authors.

Notes on contributors

Dr Shahram Derakhshan is an assistant professor at School of Mechanical Engineering, Iran University of Science and Technology, researching on environmental fluid mechanics, fluid machinery and renewable energy.

Mr Ahmad Shaker is a research assistant at School of Mechanical Engineering, Iran University of Science and Technology, researching on natural ventilation in buildings.

References

ANSYS. (1998). *ANSYS fluent 12 user's guide 2012*. Lebanon: Fluent Inc.

Allard, F. (1998). *Natural ventilation in buildings: A design handbook*. London: James and James Ltd.

Allocca, C., Chen Q., Glicksman L. (2003). Design analysis of single-sided natural ventilation. *Energy and Buildings*, *35*, 785–795.

Andersen, K. (2015). Semi-empirical models for buoyancy-driven ventilation - a literature study. *International Journal of Ventilation*, *14*, 77–90.

Bartzanas, T., Kittas, C, & Nikita-Martzopoulou, C. (2007). Analysis of airflow through experimental rural buildings: Sensitivity to turbulence models. *Biosystems Engineering 97*, 229–239.

Blocken, B., Carmeliet, J., & Stathopoulos T. (2007). CFD evaluation of the wind speed conditions in passages between buildings-effect of wall-function roughness modifications on the atmospheric boundary layer flow. *Wind Engineering and Industrial Aerodynamics*, *95*, 941–962.

Blocken, B., Stathopoulos. T., & Carmeliet, J. (2007), CFD simulation of the atmospheric boundary layer: Wall function problems. *Atmos Environ, 41*, 238–252.

Cebeci, T., & Bradshaw, P. (1977). *Momentum transfer in boundary layers*. New York, NY: Hemisphere Publishing Corp.

Chu, C., & Chiang, B. (2013). Wind-driven cross-ventilation with internal obstacles. *Energy and Buildings, 67*, 201–209.

Chu, C., and Chiang, B. (2014). Wind-driven cross ventilation in long buildings. *Building and Environment*, 80, 150–158.

Chu. C., Chiu, Y., Chen, Y., Wang Y., & Chou, C. (2009). Turbulence effects on the discharge coefficient and mean flow rate of wind-driven cross ventilation. *Building and Environment*, *44*, 2064–2072.

Chu, C., Chiu, Y., & Wang, Y. (2010). An experimental study of wind-driven cross ventilation in partitioned buildings. *Energy and Buildings, 42*, 667–673.

Etheridge, D. (2012). *Natural ventilation of buildings: Theory and measurement and design*. Chichester: John Wiley and Sons.

Etheridge. D., & Sandberg, M. (1996). *Building ventilation: Theory and measurement*. Chichester: John Wiley & Sons.

Fatnassi, H., Boulard, T., Poncet, C., & Chave, M. (2006). Optimisation of greenhouse insect screening with computational fluid dynamics. *Biosystems Engineering, 93*, 301–312.

Franke, J., Hellsten, A,, Schlünzen. H., & Carissimo, B. (2007). *Best practice guideline for the CFD simulation of flows in the urban environment*. Brussels: COST Office.

Ghadiri, M.H., Lukman, N., & Mohamed, F. (2013). Computational analysis of wind-driven natural ventilation in a two sided rectangular wind catcher. *International Journal of Ventilation, 12*, 51–62.

Hathway, A., Papakonstantis, I., Bruce-Konuah, A., & Brevis, W., (2015). Experimental and modelling investigations of air exchange and infection transfer due to hinged-door motion in office and hospital settings. *International Journal of Ventilation*, 14, 127–140.

Hu, C.H., Ohba, M., & Yoshie, R. (2008). CFD modelling of unsteady cross ventilation flows using LES. *Wind Engineering and Industrial Aerodynamics*, *96*, 1692–1706.

Jesson, M., Sterling, M., Letchford, C., & Baker. C. (2015). Aerodynamic forces on the roofs of low-, mid- and high-rise buildings subject to transient winds. *Wind Engineering & Industrial Aerodynamics 143*, 42–49.

Jiang, Y., Alexander, D., Jenkins, H., Arthur, R., & Chen, Q., (2003). Natural ventilation in buildings: measurement in a wind tunnel and numerical simulation with large-eddy simulation. *Wind Engineering and Industrial Aerodynamics*, *91*, 331–353.

Jiang, Y., & Chen, Q. (2001). Study of natural ventilation in buildings by large eddy simulation. *Wind Engineering and Industrial Aerodynamics, 89*, 1155–1178.

Jiang, Y., & Chen, Q. (2002). Effect of fluctuating wind direction on cross natural ventilation in buildings from large eddy simulation. *Building and Environment*, *37*, 379–386.

Karava, P. (2008). Airflow prediction in buildings for natural ventilation design: Wind tunnel measurements and simulation. PhD Thesis, Concordia University.

Karava, P., & Stathopoulos, T. (2012). Wind-induced internal pressures in buildings with large façade openings. *Journal Eng Mech*, *138*, 358–370.

Karava, P., Stathopoulos, T., & Athienitis, A. (2004). Wind driven flow through openings - a review of discharge coefficients. *International Journal of Ventilation, 3*, 255–266.

Karava, P., Stathopoulos, T., & Athienitis, A. (2006). Impact of internal pressure coefficients on wind-driven ventilation analysis. *International Journal of Ventilation, 5*, 53–66.

Karava, P., Stathopoulos, T., & Athienitis, A. (2011). Airflow assessment in cross ventilated buildings with operable façade elements. *Building and Environment, 46*, 266–279.

Kato, S., Murakami S., Mochida A., Akabayashi S., & Tominaga, Y. (1992). Velocity-pressure field of cross ventilation with open windows analyzed by wind tunnel and numerical simulation. *Wind Engineering & Industrial Aerodynamics*, *44*, 2575–2586.

Larsen, T.S., Nikolopoulos, N., Nikolopoulos, A., Strotos G., & Nikas, K.S. (2011). Characterization and prediction of the volume flow rate aerating a cross ventilated building by means of experimental techniques and numerical approaches. *Energy and Buildings, 43*, 1371–1381.

Launder, B., & Spalding, D. (1974). The numerical computation of turbulent flows. *Computer Methods Applied Mech Eng*, *3*, 269–289.

Lee, I., Lee, S., Kim, G., Sung, J., Sung, S., & Yoon, Y. (2005). PIV verification of greenhouse ventilation air flows to evaluate CFD accuracy. *Trans ASAE, 48*, 2277–2288.

Linden, P. (1993). The fluid mechanics of natural ventilation. *Annual Review Fluid Mech 31*, 201–238.

Liu, X., Niu, J., & Kwok, K. (2011). Analysis of concentration fluctuations in gas dispersion around high-rise building for different incident wind directions. *Hazardous Materials, 192*, 1623–1632.

Menter, F.R. (1994). Two-equation eddy-viscosity turbulence models for engineering applications. *AIAA Journal*, *32*, 1598–1605.

Mistriotis, A., Bot, G., Picuno, P., & Scarascia-Mugnozza, G. (1997). Analysis of the efficiency of greenhouse ventilation using computational fluid dynamics. *Agric For Meteorol*, *85*, 217–228.

Montazeri H., & Blocken, B. (2013). CFD simulation of wind-induced pressure coefficients on buildings with and without balconies: Validation and sensitivity analysis. *Building and Environment, 60*, 137–149.

Murakami, S., Kato, S., Akabayashi, S.M.K., & Kim, Y. (1991). Wind tunnel test on velocity pressure field of cross-ventilation with open windows. *ASHRAE Trans*, *97*, 525–538.

Ohba, M., Irie, K., & Kurabuchi, T. (2001). Study on airflow characteristics inside and outside a cross-ventilation model, and ventilation a flow rates using wind tunnel experiments. *Journal of Wind Engineering and Industrial Aerodynamics*, *89*, 1513–1524.

Orme, M. (2001). Estimates of the energy impact of ventilation and associated financial expenditures. *Energy and Buildings, 33*, 199–205.

Patankar, S. (1980). *Numerical heat transfer and fluid flow*. New York, NY: Taylor & Francis.

Peren, J.I., van Hooff, T., Leite, C,, & Blocken, B. (2015). CFD analysis of cross-ventilation of a generic isolated building with asymmetric opening positions: Impact of roof angle and opening location. *Building and Environment*, *85*, 263–276.

Ramponi, R., & Blocken, B. (2012a). CFD simulation of cross-ventilation flow for different isolated building configurations: Validation with wind tunnel measurements and analysis of physical and numerical diffusion effects. *Wind Engineering & Industrial Aerodynamics*, 408–418.

Ramponi, R., & Blocken, B. (2012b). CFD simulation of cross-ventilation for a generic isolated building: Impact of computational parameters. *Building and Environment, 53*, 34–48.

Rong, L., Liu, D.,, Pedersen, E., & Zhang, G. (2015). The effect of wind speed and direction and surrounding maize on hybrid ventilation in a dairy cow building in Denmark. *Energy and Buildings, 86*, 25–34.

Saha, C., Ammon, C., Berg, W., Loebsin, C., Fiedler, M., Brunsch, R,, & Von Bobrutzki, K. (2013). The effect of external wind speed and direction on sampling point concentrations, air change rate and emissions from a naturally ventilated dairy building. *Biosystems Engineering*, *114*, 267–278.

Seifert, J., Li, Y., Axley, J., & Rösler, M. (2006). Calculation of wind-driven cross ventilation in buildings with large openings. *Wind Engineering & Industrial Aerodynamics*, *94*, 925–947.

Stephen D.R., & Leon, R.G. (2013). Increased natural ventilation flow rates through ventilation shafts. *International Journal of Ventilation, 12*, 195–209.

Tominaga. Y., & Blocken, B. (2015). Wind tunnel experiments on cross-ventilation flow of a generic building with contaminant dispersion in unsheltered and sheltered conditions. *Building and Environment*, *92*, 452–461.

Tominaga, Y., Mochida, A., Yoshie, R., Kataoka, H., Nozu, T., Yoshikawa, M., & Shirasawa, T. (2008). AIJ guidelines for practical applications of CFD to pedestrian wind environment around buildings. *Wind Engineering and Industrial Aerodynamics, 96*, 1749–1761.

Tominagaa, Y., Akabayashib, S., Kitaharaa, T., & Arinamib, Y. (2015). Air flow around isolated gable-roof buildings with different roof pitches: Wind tunnel experiments and CFD simulations. *Building and Environment*, *84*, 204–213.

Van Hooff, T., & Blocken, B. (2010). Coupled urban wind flow and indoor natural ventilation modelling on a high-resolution grid: A case study for the Amsterdam ArenA stadium. *Environmental Modelling & Software, 25*, 51–65.

Wong, N., Hand Heryanto, S. (2004), The study of active stack effect to enhance natural ventilation using wind tunnel and computational fluid dynamics (CFD) simulations. *Energy and Buildings, 36*, 668–678.

Yu, X.F., Xie, Z.N., & Gu, M. (2015). Interference effects on wind pressure distribution between two high-rise buildings. *Wind Engineering and Industrial Aerodynamics, 142*, 188–197.